Cell motility and drug gradients in the emergence of resistance to chemotherapy

Amy Wu[a], Kevin Loutherback[b], Guillaume Lambert[c], Luis Estévez-Salmerón[d], Thea D. Tlsty[d], Robert H. Austin[e,1], and James C. Sturm[a]

[a]Princeton Institute for the Science and Technology of Materials, Department of Electrical Engineering, Princeton University, Princeton, NJ 08544; [b]Earth Sciences Division, Lawrence Berkeley National Laboratory, Berkeley, CA 94720; [c]Department of Molecular Genetics and Cell Biology, University of Chicago, Chicago, IL 60637; [d]Department of Pathology, University of California, San Francisco, San Francisco, CA 94122; and [e]Department of Physics, Princeton University, Princeton, NJ 08544

Contributed by Robert H. Austin, August 2, 2013 (sent for review April 23, 2013)

The emergence of resistance to chemotherapy by cancer cells, when combined with metastasis, is the primary driver of mortality in cancer and has proven to be refractory to many efforts. Theory and computer modeling suggest that the rate of emergence of resistance is driven by the strong selective pressure of mutagenic chemotherapy and enhanced by the motility of mutant cells in a chemotherapy gradient to areas of higher drug concentration and lower population competition. To test these models, we constructed a synthetic microecology which superposed a mutagenic doxorubicin gradient across a population of motile, metastatic breast cancer cells (MDA-MB-231). We observed the emergence of MDA-MB-231 cancer cells capable of proliferation at 200 nM doxorubicin in this complex microecology. Individual cell tracking showed both movement of the MDA-MB-231 cancer cells toward higher drug concentrations and proliferation of the cells at the highest doxorubicin concentrations within 72 h, showing the importance of both motility and drug gradients in the emergence of resistance.

Cancer cells evolve drug resistance to chemotherapy within the tumor microenvironment. Although it is widely accepted that the tumor microenvironment provides a sequential selective pressure for preexisting mutants within the population (1–3), an additional contribution to rapid cancer evolution is mutagenic stress response followed by the emergence of adaptive phenotypes (4, 5). Further, mutagenic drug gradients in the tumor microenvironment lead to a spatially dependent fitness landscape of the cancer cells and can further accelerate the evolution of drug resistance if the cells are motile across the gradient (5, 6). We recently demonstrated using a bacteria model how a spatial gradient of antibiotic concentration in a metapopulation accelerated the evolution of antibiotic resistance (7). We would expect similar processes to occur in cancer cell metapopulations as well. Because cancer cells have a much longer doubling time (~1 d) compared with that of bacteria (~30 min), similar experiments with cancer cells take an order of magnitude more time (days vs. hours) than those for bacteria. This presents two experimental challenges: (*i*) creation of a drug stable gradient and (*ii*) creation of an environment hospitable for healthy cell growth. Once these conditions are established, it is possible to probe in an in vitro system the complex driving forces of resistance in systems that are in vivo.

Results

Microfluidic devices have become a versatile platform to provide precise concentration gradient control for understanding various biological systems and controlling the population size (8–10). Gradient-generating devices can be classified as (*i*) static generators, which are based solely on diffusion (11, 12), and (*ii*) constant-flow generators (13–16). In this paper we adopt the constant-flow approach because it is capable of creating time-independent stable gradients. However, to date, it has been challenging to grow mammalian cells in such platforms (17, 18). Thus, the time scale of previous studies of breast cancer chemotaxis in a gradient of epidermal growth factors was limited to 24 h (19). In this paper we develop a microfluidic platform for the long-term (multiday) culture of metastatic breast cancer cells (MDA-MB-231) in a stable gradient.

We work with a putative metastatic breast cancer cell line (MDA-MB-231) instead of nonmetastatic breast cancer cells (such as MCF-7). The MDA-MB-231 cell line is a highly aggressive, invasive, and poorly differentiated human breast cancer cell line with a mesenchymal rather than an epithelial phenotype (20). A further consideration in using the MDA-MB-231 cell line is the connection between metastasis, motility, and metabolic energy consumption. Metastatic breast cancer MDA-MB-231 uses the aerobic glycolysis, compared with the usual mitochondrial oxidative phosphorylation cycle, consuming glucose less efficiently in terms of ATP production but more efficiently in storage of chemical energy (21, 22). Although cancer invasion and resistance have been discussed separately for a long time, the two phenotypes reveal substantial overlaps on bimolecular pathways and demand in energy consumption. Induced by metabolic stresses such as nutrient deficiency or hypoxia, cell adhesion, growth, and survival signal are altered in a tumor microenvironment. The stabilization of hypoxia-inducible factor 1 adjusts cell metabolism toward glycolysis (the Warburg effect) and increases the expression of multidrug resistance proteins, such as P-gp (23). The metabolic drug efflux pump, a major mechanism of drug resistance, further consumes a large amount of energy via glycolysis (24). Therefore, a feed-forward phenomenon regarding the Warburg cycle may be able to explain the interconnection of cancer motility and emergence of drug resistance in a drug gradient. Thus, MDA-MB-231, which presents a glycolytic phenotype, was our choice for this study.

Perfusion Rather Than Direct Flow Necessary for MDA-MB-231 Culture. We found that a necessary condition for successful long-term (16-d) MDA-MB-231 cell culture is the absence of any continuous fluid flow above 1 μm/s in the culture region, which led us to the cross-channel perfusion device architecture (discussed further in

Significance

Ultimately, chemotherapy often fails because of the emergence of cancer cells resistant to the chemotherapy. We show that this emergence can be driven by the presence of chemotherapy drug gradients and motility of the cancer cells within the gradient.

Author contributions: A.W., K.L., G.L., L.E.-S., T.D.T., R.H.A., and J.C.S. designed research; A.W. performed research; K.L., G.L., and L.E.-S. contributed new reagents/analytic tools; A.W., R.H.A., and J.C.S. analyzed data; and A.W., T.D.T., R.H.A., and J.C.S. wrote the paper.

The authors declare no conflict of interest.

Freely available online through the PNAS open access option.

[1]To whom correspondence should be addressed. E-mail: austin@princeton.edu.

This article contains supporting information online at www.pnas.org/lookup/suppl/doi:10.1073/pnas.1314385110/-/DCSupplemental.

Downloaded at Palestinian Territory, occupied on December 14, 2021

MEDICAL SCIENCES

ENGINEERING

www.manaraa.com

Materials and Methods and Figs. S1 and S2). A cross-channel diffuser gradient device can generate stable gradients with low fluid flow rate in the culture region (15, 25). We developed a cross-channel diffuser approach for long-term cell culture. This device separates the culture chamber (1 mm × 1 mm, with a depth of 150 μm in our case) from the flow channels on opposing sides of the chamber, one of which supplies the drug and the second of which has a flow of media free of the drug. These two channels are separated from the culture region by a linear array of microposts, which have narrow gaps of 5 μm between them. The arrays of posts serve as a perfusion barrier, which allows the drug to diffuse through the gaps between the posts but does not allow a substantial fluid flow from the source and sink channels through the gaps into the culture chamber (Fig. 1 *A* and *B*). To ensure that there is no flow in the culture chamber, the external connections through the left and right ends (inlet and outlet for cell loading) are closed during cell culture.

Using continuous source and sink flow in the outer channels with an average flow rate of 100 μm/s (supplied by syringe pumps), the resulting gradient profile was linear when tested using fluoroscein, which has a similar diffusion coefficient to and can thus be used as a substitute for doxorubicin. By maintaining a constant flow in the outer source and sink channels, the gradient was very stable (Fig. 1 *D* and *E*). In contrast to static gradient devices in which there is no flow to refresh the source and sink regions outside the culture region (11, 12), in these devices the gradients can, in principle, be maintained indefinitely. To measure fluid flow speeds, in one case we added fluorescent beads to the input media. In the culture chamber, we found that the fluid flow speed was less than 1 μm/s, over 100 times lower than in the side channels and comparable to physiologic level of interstitial flow, about 0.5 μm/s (Fig. 1*C*) (26).

In a control experiment without any drugs (flowing fresh growth media in both the source and sink channels), the MDA-MB-231 cells grew well in the chip for more than 2 wk (Fig. 2*A*). The cells showed healthily elongating morphologies and became more confluent with time. The growth curves of the cells (Fig. 2*B*) show that the cells grew in a log phase for 4 d with doubling times of 2.2 d (in chips) and 2 d (in tissue culture flasks) and then entered the stationary phase, where they remained for the rest of the 2 wk. Creating such a hospitable environment for the cancer cells on the microchips was an experimental challenge, the critical steps for which are described in more detail in *Materials and Methods*.

Population Dynamics of Breast Cancer Cell Adaptation in a Microenvironment with Drug Gradients. Doxorubicin is a genotoxic chemotheraputic drug; unfortunately, the literature IC_{50} (drug concentration that inhibits the viability of 50% of population in a drug-free control) of doxorubicin for MDA-MB-231 cells varies from 25 nM to 88 nM to 2.7 μM (27–29). Thus, to find the desired dosage for our gradient experiments, we compared the effects of different doxorubicin concentrations on our MDA-MD-231 cell line for multiple days in tissue culture flasks (Fig. 3). We found that 200 nM doxorubicin effectively inhibited the growth of MDA-MB-231 after 24 h and also induced morphological changes in 96 h (Fig. 3 *A* and *B*), and we chose this value for the concentration for the input stream for the channel on the source side of the culture chamber. Thus, after loading the cells into the culture chamber of our gradient device and after a 24-h attachment period, a doxorubicin gradient was constructed by pumping 200 nM doxorubicin at the source channel and pumping growth medium alone at the sink channel.

Doxorubicin is a genotoxic drug which damages the chromatin of cells; this was shown in cells exposed to 200 nM doxorubicin in the chip. After 72 h, we used a single-cell gel electrophoresis assay (SCGE) and observed an average tail moment length of 27 μm (Fig. 3*C*). In this assay, broken DNA migrates farther in the electric field, resulting in a comet tail. We show that 72-h exposure of 200 nM doxorubicin is adequate to induce significant DNA

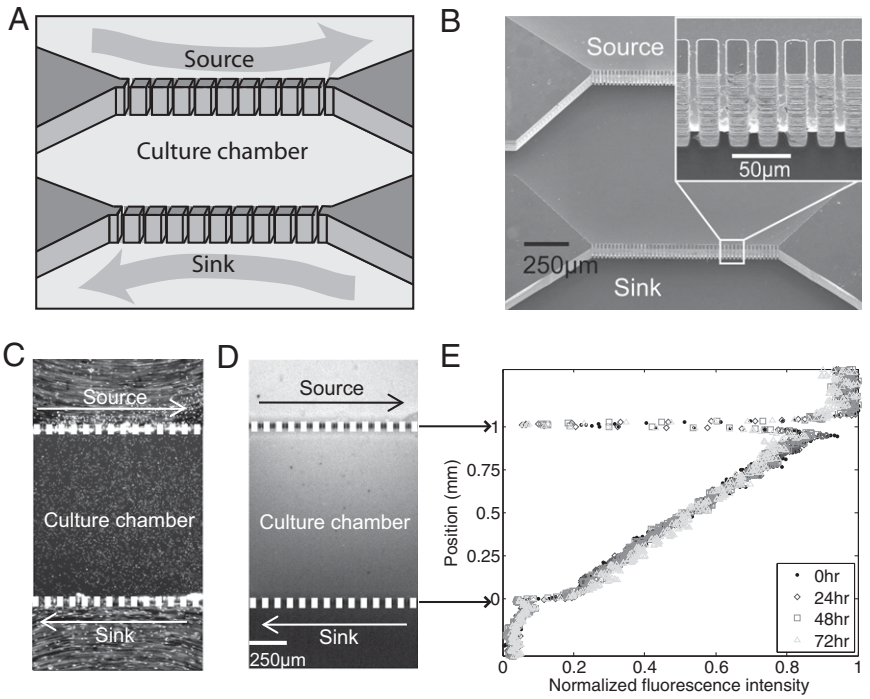

Fig. 1. Cross-channel diffuser design and gradient characterization. (*A*) Schematic of the cross-channel device. (*B*) Scanning electron microscopic image of the cross-channel device etched into silicon (depth is 150 μm). The gap between the microposts (20 μm × 40 μm) is 5 μm. The source and sink channels were 3 mm wide. (*C*) Characterization of flow speeds using fluorescent beads (diameter is 1 μm). Exposure time is 2 s. (*D*) Fluorescent micrograph of fluorescein gradient, with source and sink flow rates of 100 μm/s. (*E*) Gradient profile across the culture chamber.

Downloaded at Palestinian Territory, occupied on December 14, 2021
www.manaraa.com

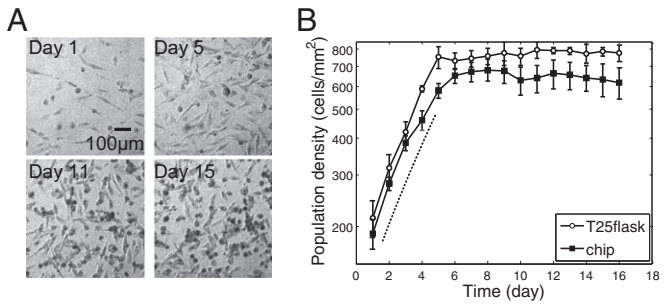

Fig. 2. Control experiments of MDA-MB-231 cells in the cross-channel mixer without drug. (*A*) Micrographs of MDA-MB-231 cells in the culture chamber of the cross-channel device in time series from day 1 to day 15. (*B*) Growth curves of MDA-MB-231 cells in the culture chamber of the cross-channel mixer vs. conventional tissue culture flask. In the mixer, the flow rate in the source and sink channels was 100 μm/s. For the flasks, the medium has been replaced every 4 d. The doubling time is 2.2 d in the chips and 2 d in tissue culture flasks. Error bars represent the SD of three replicates.

damage in MDA-MB-231 cells. The resulting distribution of cells was imaged using bright-field microscopy every 25 min over 72 h.

Fig. 4*A* shows the image of cells in the growth chamber at 0 h (defined as after the 24-h attachment period). Qualitatively, after 72 h with the applied gradient, the cell density increased throughout the culture chamber, under all drug concentrations, and not surprisingly increased faster in the lower half (low-drug region) of the culture chamber (Fig. 4*B*). To quantify the population vs. space and time, we divided the culture chamber into five regions of interest along the gradient direction, with drug concentrations from top to bottom of 200–160 nM, 160–120 nM, 120–80 nM, 80–40 nM, and 40–0 nM, indicated by the dotted lines. The cell density was initially uniform in the five regions (between 260 cells per mm^2 and 300 cells per mm^2); after 24 h the cell population increased more significantly in the low-drug region than in the high-drug region, forming a population gradient in response to the drug gradient (Fig. 4*B*). Most surprisingly, the cell population in the high-drug region (160–200 nM) began to increase significantly after only 48 h. It is also instructional to plot the cell density in each drug concentration region vs. time (Fig. 4*C*). One notes that in the low-drug region, cells grow continuously from the beginning of the experiment, whereas in regions of increasingly higher drug concentration, there is a delay until the cell population starts growing. The delay increases with the drug concentration. Over the range of time for which we have data, after the delay, to first order the growth rates in all drug concentration regions are similar.

There are three possible ways that cancer cells in a fitness landscape can show growth at levels of a drug which should inhibit growth: (*i*) The first scenario is long-range random migration. If the cancer cells were to migrate rapidly and randomly on a length scale as large as the culture chamber in a drug gradient, they would survive longer in a high-drug region than in a uniform high-drug environment because they would only spend a short portion of their life in the high-drug region. (*ii*) The second scenario is long-range directed motion to regions of higher stress as resistance emerges. Conventional chemotaxis would be expected to drive the cells away from the high-drug region. However, from a fitness advantage perspective it is advantageous for a cell to move toward regions of higher stress if resistance emerges because of reduced competition for resources such as glucose, oxygen, or space (22). (*iii*) The third scenario is local evolution of resistance to the drug without any influence of migration of the cells. In this case the cells should show proliferation in the high-drug region.

To test these hypotheses, we first analyzed the trajectories of 12 individual cells at different positions within the doxorubicin gradient. Fig. 5*A* shows the local trajectories of the individual cells over time. The information to be extracted here is that there

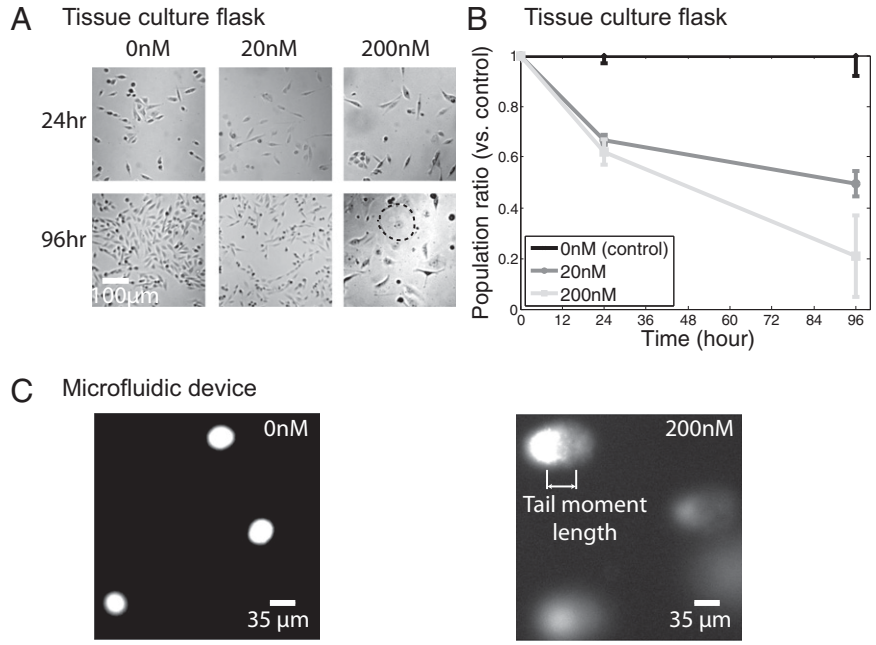

Fig. 3. MDA-MB-231 cells in various concentrations of doxorubicin. (*A*) Micrographs of MDA-MB-231 exposed to 0 nM, 20 nM, and 200 nM doxorubicin for 24 h or 96 h in the tissue culture flasks. Under 200 nM doxorubicin, the cell growth was effectively inhibited in 24 h, and cells became large and flattened significantly in 96 h (for example, the cell circled by the dotted line). (*B*) Population ratio to control experiment (0 nM) vs. time in the tissue culture flasks. Error bars represent the SD of three replicates. After ~48-h exposure, 200 nM doxorubicin inhibits 50% of cells (IC_{50}). (*C*) DNA damage (comet assay) of the cells from the microfluidic mixer after 72-h doxorubicin exposure (0 nM vs. 200 nM). Fifteen cells have been analyzed in each concentration. The tail moment lengths are 0 μm and 27.0 ± 8.4 μm for 0 nM and 200 nM, respectively.

Downloaded at Palestinian Territory, occupied on December 14, 2021
MEDICAL SCIENCES
ENGINEERING
www.manaraa.com

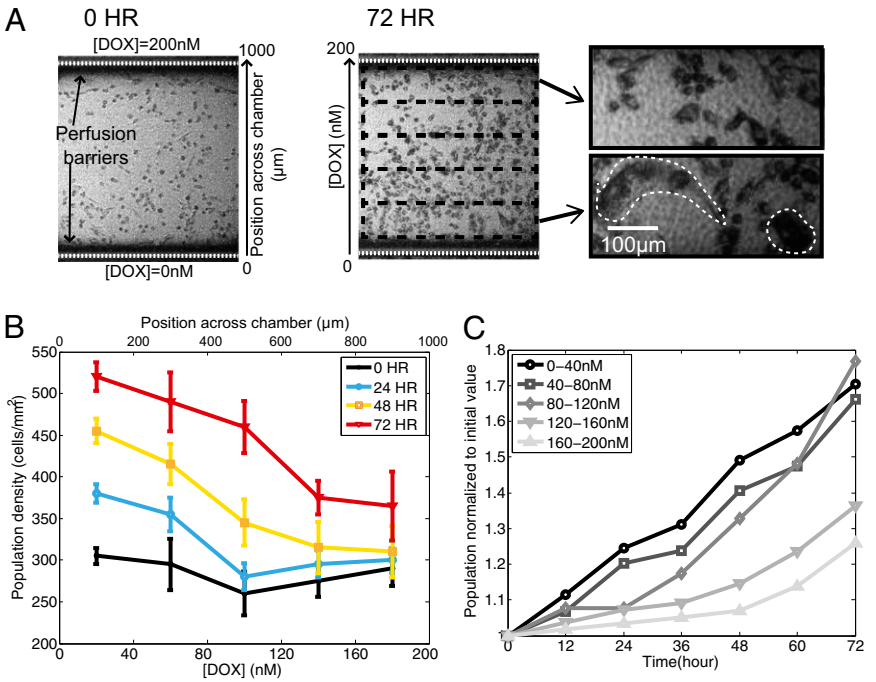

Fig. 4. MDA-MB-231 cells (0–72 h) under doxorubicin gradient (200 nM/mm). (*A*) Micrographs of the cells. The rows of the posts separating the culture chamber from the source channel (top) and sink channel (bottom) have been artificially added to the image for clarity. The source channel contains 200 nM doxorubicin, and the sink channel has 0 nM. The 72-h image has schematically indicated five regions for different drug concentrations for counting cells. The cell morphologies at the high-drug region (160–200 nM) and the low-drug region (0–40 nM) are compared. We observed some enlarged cells at the low-drug region, circled by dotted lines. (*B*) Cell population density in five regions of the culture chamber vs. time. Error bars represent SD of the data within 100 min of each time point, indicating the temporal variation due to cell migration and division. (*C*) Normalized growth curves in different regions of interest. Each curve is normalized by its initial value.

is no obvious bias to the motions of the cells vs. position in the gradient and that you must integrate the positions and the cells in different regions vs. time to address the three hypotheses that we posed above. Fig. 5*B* shows the integrated displacements, averaged over cells in the region, vs. time. It is clear that the cells do not move from the drug and that they do not move over significant distances greater than the total 1,000-μm width of the drug gradient, but there is a biased movement toward the higher doxorubicin drug levels. The significance analysis is described in more detail in *Materials and Methods*.

To gain information on whether the cells acquired division capability in the high-drug region, we characterized the cell divisions in each bin in the drug gradient vs. time. We count the number of cell divisions using tracking software developed by Danusers laboratory (30). Then we define the cell proliferation rate as the accumulated number of cell divisions in each bin divided by the initial cell population in each 12-h time span in each bin. We show the deviation of cell proliferation rate in each bin from the average proliferation rate over the entire culture chamber (Fig. 6). We find that the peak of the deviation of cell proliferation rate spreads from the low-drug region to the high-drug region with time. The cells in the high-drug region gradually acquired greater division capability than those in the low-drug region with time.

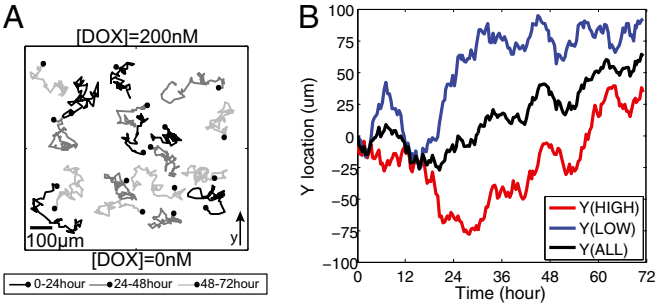

Fig. 5. MDA-MB-231 cell migration in a doxorubicin gradient (200 nM/mm). (*A*) Movement of selected cancer cells in the doxorubicin gradient tracked over three time intervals. (*B*) Integrated net displacement in the *y* direction (the drug gradient axis) for cells in the upper and lower drug gradient and the net overall displacements for 12 individual cells.

Discussion

We have shown that stable long-term drug gradients can be engineered into a cell culture region with microfluidic methods and that MDA-MB-231 cells can be successfully cultured for over 2 wk in these on-chip environments without drugs. With a strong drug gradient applied (200 nM to 0 nM over 1 mm) to the culture chamber, the population density increases, even in regions of high drug concentration. This population increase was not due to the fact the cells spent only a small fraction of their lives in the high-drug regions due to random motion. Instead, the cells migrated in a biased random motion toward the drug source because of reduced competition for resources.

The competition for resources may be a combination of (*i*) space, due to contact inhibition of adherent cells, and (*ii*) metabolic resources, such as glucose or oxygen. The first factor is obvious, but one may ask whether the rate of resource consumption exceeds the rate of resource replenishment by constant perfusion. Although we apply constant perfusion in cross-channel diffuser, cell-secreted growth factors may not be rinsed away as in the premixer (Figs. S1 and S2) because the cells grow well in cross-channel diffuser (Fig. 2). It is possible that each cell becomes a local sink of metabolic resources and creates microheterogeneities in resource concentrations that can be detected by neighboring cells. The propagation of cell proliferation vs. time also suggests that the growth of cells in low-drug regions

Downloaded at Palestinian Territory, occupied on December 14, 2021
www.manaraa.com

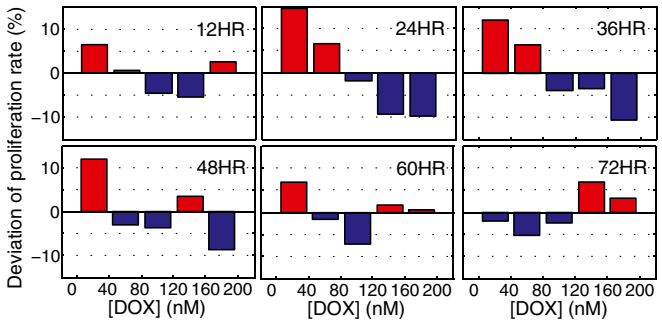

Fig. 6. Deviation of cell proliferation rate per 12 h (in each bin) from cell division percentage of the entire chamber vs. time. We count the number of cell divisions in each bin over every 12-h period from 0 h to 72 h. The cell proliferation rate is defined as number of cell divisions divided by the initial population. Here we show the deviation of cell proliferation rate in each bin from the average cell proliferation rate over the entire chamber.

confers an advantage to cells in adjacent regions with higher drug concentration.

Materials and Methods

Exposed Flow Premixer Design. Besides the perfusion barrier approach to creating a controlled gradient, we also tested the premixer approach in which six premixed streams (200 μm wide) of increasing drug concentrations flow parallelly into a 1.2-mm-wide culture chamber adjacent to one another (Fig. S1*A*). Subsequent diffusion causes the boundaries between the streams to be blurred and create a smooth gradient in the culture chamber (Fig. S1*B*). The concentration profiles can be maintained down through the culture chamber if the flow speed is fast enough (i.e., $v >$ 3 mm/s) (Fig. S1*C*). If the flow speed is too slow, however, (i.e., $v < 0.1$ mm/s), diffusion flattens the concentration profiles as the liquids move along the culture chamber (Fig. S1*D*), and the gradient is lost.

The minimum flow rate requirement is significant because we found that even with zero drug concentration (only fresh media flowing in the culture region in all channels), fluid flows as low as 8 μm/s in the culture region would adversely affect the growth of MDA-MB-231 cells. After 48 h without flow, MDA-MB-231 cells in the culture chamber showed a healthily elongated morphology (Fig. S2*A*, *Top*), but under 16 μm/s of flow (from 24 to 48 h), the cancer cells became round and blebbing (Fig. S2*A*, *Bottom*). Furthermore, the population under flow decreased in 72 h because the cells were detached and flushed away by the flow, even at a flow speed of only 8 μm/s (Fig. S2*B*). One reason that the cells grew poorly under a continuous flow may be the loss of secreted growth factors (8), although replacing the fresh medium with conditioned media did not substantially alter the results (Fig. S2*C*). More complicated mechanisms such as flow-mediated mechanotransduction also explain the disruption of cell growth by shear stress (31).

Device Fabrication and Flow Characterization. The cross-channel device (150 μm deep) was made by reactive ion etching of silicon (RIE800iPB; Samco Inc.) using standard photolithography technology. Then holes were sandblasted through the substrate so that fluidics could flow from the bottom of the substrate to the device on the top surface. The top of the device was reversibly sealed by a poly(dimethylsiloxane) (PDMS)-coated glass slide clamped by an acrylic manifold allowing input and output of liquids. The premixer device was molded in PDMS from a 120-μm-deep silanized silicon mold etched by reactive ion etching (RIE800iPB; Samco Inc.) using standard soft lithography techniques (32). After punching the ports of the inlet and outlet with biopsy needles, the PDMS device was permanently bonded to a glass slide via oxygen plasma treatment. A syringe pump with two syringes was used to supply a continuous flow to the two inlets.

The concentration gradient of the device was observed by continuously pumping growth medium dissolved with sodium fluorescein (Sigma-Aldrich) at inlet 1 and growth medium alone at inlet 2 using a syringe pump (Chemyx Inc.). The diffusion coefficient of sodium fluorescein ($D = 4.04 \times 10^{-10}$ m^2/s) is similar to that of doxorubicin ($D = 3.58 \times 10^{-10}$ m^2/s), a common chemotherapeutic drug. The diffusion coefficients were calculated based on their molecular weights (33). The flow speed in the culture chamber was measured by pumping fluorescent polystyrene beads (with a diameter of 1 μm) into source and sink channels and then tracking the bead trajectories from the image with an exposure time of 2 s.

On-Chip Cell Culture. The MDA-MB-231 breast cancer cells were provided by T.D.T.'s laboratory (University of California, San Francisco) and were cultured in a growth medium (DMEM supplemented with 10% (vol/vol) FBS, 1% penicillin-streptomycin) in an incubator with 5% CO_2 set to 37°C. The growth medium was prewarmed in an incubator to reach equilibrium prior to use. The silicon cross-channel mixer was coated with fibronectin (6 μg/μm^2) before cell seeding. The suspended cells were then gently seeded into the microfluidic device via the cell inlet at a density of 2 million cells per mL and were allowed to attach to the substrate by overnight incubation. After 24 h of static incubation, the growth medium and the drug solution were supplied continuously. The premixer device was coated by incubation with 0.1% gelatin for 1 h to promote cell attachment onto the glass substrate. After removing the gelatin solution, the culture chamber was filled with growth medium.

Image Acquisition and Analysis. The cells in the device were observed by acquiring epi–bright-field images every 5 min using a compound microscope [with a white light-emitting diode, dichroic mirror, 4× objective, and a complementary metal–oxide–semiconductor (CMOS) camera (Thorlabs, Inc.)]. The entire device, the syringe pump to supply the growth medium and drugs (if any), and the imaging system were placed inside a conventional incubator with 5% CO_2 set to 37°C. The cell population was determined by threshold-based automatic counting software (MATLAB) that was calibrated with manual counting.

Characterization of DNA Damage. The OxiSelect Comet Assay Kit (Cell Biolabs, Inc.), a SCGE, was used to quantify the DNA fragmentation of the cells induced by doxorubicin. After 72 h of doxorubicin exposure, the cells were collected by scraping them from the microfluidic device with a rubber policeman. The cells were then combined with agarose and treated with a lysis buffer and alkaline solution to relax and denature the DNA. Finally, the samples were electrophoresed to separate the intact DNA from damaged fragments. By staining with a DNA fluorescent dye, the migration of the damaged DNA (a "comet tail") was visualized by an epifluorescence microscope.

Significance Analysis. The following significance test for a drift toward the high-drug region was carried out: Based on the 72-h trajectories for the 12 individual cells, 9 out of 12 cells migrated toward the high-drug region (with final Y displacement greater than 0). We design a significance test based on a binomial distribution, $B(n,p)$, where n is the cell counts and p is the probability of cells migrating toward the high-drug region (with final Y displacement greater than 0). If there is no significant drift toward the high- or low-drug region, p should be equal to 0.5.

The null hypothesis (H_0) states that $p_0 = 0.5$, and unbiased random walk dominates the cell migration in the doxorubicin gradient.

The alternative hypothesis (H_1) states that $p_0 = 0.5$, and there is a bias in cell migration in the doxorubicin gradient.

Let n_1 be the number of cells that migrated toward the high-drug region, n is the total number of tracked cells, and $p = n_1/n = 9/12 = 0.75$. The 95% confidence interval based on the Wald method is $[p - 1.96\sqrt{p(1-p)/n}, p + 1.96\sqrt{p(1-p)/n}] = (1.505, 0.995)$. The null value p_0 is not in the 95% confidence interval. Thus, there is a bias of cell motion in Y direction toward the high-drug region during the 72-h period.

ACKNOWLEDGMENTS. We thank Liyu Liu and Henrik Flyvbjerg for helpful discussions. This project was supported primarily by the National Cancer Institute. This work was supported in part by the National Science Foundation under Grant PHYS-1066293 and the hospitality of the Aspen Center for Physics.

1. Bozic I, et al. (2010) Accumulation of driver and passenger mutations during tumor progression. *Proc Natl Acad Sci USA* 107(43):18545–18550.
2. Leder K, et al. (2011) Fitness conferred by BCR-ABL kinase domain mutations determines the risk of pre-existing resistance in chronic myeloid leukemia. *PLoS ONE* 6(11):e27682.
3. Greaves M, Maley CC (2012) Clonal evolution in cancer. *Nature* 481(7381):306–313.
4. Gillies RJ, Gatenby RA (2007) Adaptive landscapes and emergent phenotypes: Why do cancers have high glycolysis? *J Bioenerg Biomembr* 39(3):251–257.
5. Lambert G, et al. (2011) An analogy between the evolution of drug resistance in bacterial communities and malignant tissues. *Nat Rev Cancer* 11(5):375–382.
6. Trédan O, Galmarini CM, Patel K, Tannock IF (2007) Drug resistance and the solid tumor microenvironment. *J Natl Cancer Inst* 99(19):1441–1454.

Downloaded at Palestinian Territory, occupied on December 14, 2021
MEDICAL SCIENCES
ENGINEERING
www.manaraa.com

7. Zhang Q, et al. (2011) Acceleration of emergence of bacterial antibiotic resistance in connected microenvironments. *Science* 333(6050):1764–1767.
8. Keenan TM, Folch A (2008) Biomolecular gradients in cell culture systems. *Lab Chip* 8(1):34–57.
9. Walsh CL, et al. (2009) A multipurpose microfluidic device designed to mimic microenvironment gradients and develop targeted cancer therapeutics. *Lab Chip* 9(4): 545–554.
10. Chung BG, Choo J (2010) Microfluidic gradient platforms for controlling cellular behavior. *Electrophoresis* 31(18):3014–3027.
11. Abhyankar VV, et al. (2008) A platform for assessing chemotactic migration within a spatiotemporally defined 3D microenvironment. *Lab Chip* 8(9):1507–1515.
12. Kim D, Lokuta MA, Huttenlocher A, Beebe DJ (2009) Selective and tunable gradient device for cell culture and chemotaxis study. *Lab Chip* 9(12):1797–1800.
13. Jeon NL, et al. (2000) Generation of solution and surface gradients using microfluidic systems. *Langmuir* 16(22):8311–8316.
14. Li Jeon N, et al. (2002) Neutrophil chemotaxis in linear and complex gradients of interleukin-8 formed in a microfabricated device. *Nat Biotechnol* 20(8):826–830.
15. Paliwal S, et al. (2007) MAPK-mediated bimodal gene expression and adaptive gradient sensing in yeast. *Nature* 446(7131):46–51.
16. Cimetta E, et al. (2010) Microfluidic device generating stable concentration gradients for long term cell culture: Application to Wnt3a regulation of β-catenin signaling. *Lab Chip* 10(23):3277–3283.
17. Kim L, Toh YC, Voldman J, Yu H (2007) A practical guide to microfluidic perfusion culture of adherent mammalian cells. *Lab Chip* 7(6):681–694.
18. Regehr KJ, et al. (2009) Biological implications of polydimethylsiloxane-based microfluidic cell culture. *Lab Chip* 9(15):2132–2139.
19. Wang SJ, Saadi W, Lin F, Minh-Canh Nguyen C, Li Jeon N (2004) Differential effects of EGF gradient profiles on MDA-MB-231 breast cancer cell chemotaxis. *Exp Cell Res* 300(1):180–189.
20. Pratap J, et al. (2006) Regulatory roles of Runx2 in metastatic tumor and cancer cell interactions with bone. *Cancer Metastasis Rev* 25(4):589–600.
21. Gatenby RA, Gillies RJ (2004) Why do cancers have high aerobic glycolysis? *Nat Rev Cancer* 4(11):891–899.
22. Liu L, et al. (2013) Minimization of thermodynamic costs in cancer cell invasion. *Proc Natl Acad Sci USA* 110(5):1686–1691.
23. Bertout JA, Patel SA, Simon MC (2008) The impact of O2 availability on human cancer. *Nat Rev Cancer* 8(12):967–975.
24. Zhou M, et al. (2010) Warburg effect in chemosensitivity: Targeting lactate dehydrogenase-A re-sensitizes taxol-resistant cancer cells to taxol. *Mol Cancer* 9(1):33.
25. Mosadegh B, et al. (2007) Generation of stable complex gradients across two-dimensional surfaces and three-dimensional gels. *Langmuir* 23(22):10910–10912.
26. Shieh AC, Rozansky HA, Hinz B, Swartz MA (2011) Tumor cell invasion is promoted by interstitial flow-induced matrix priming by stromal fibroblasts. *Cancer Res* 71(3): 790–800.
27. Smith L, et al. (2006) The analysis of doxorubicin resistance in human breast cancer cells using antibody microarrays. *Mol Cancer Ther* 5(8):2115–2120.
28. Gouaz-Andersson V, et al. (2007) Ceramide and glucosylceramide upregulate expression of the multidrug resistance gene MDR1 in cancer cells. *Biochim Biophys Acta* 1771(12):1407–1417.
29. Aroui S, et al. (2009) Maurocalcine as a non toxic drug carrier overcomes doxorubicin resistance in the cancer cell line MDA-MB 231. *Pharm Res* 26(4):836–845.
30. Jaqaman K, et al. (2008) Robust single-particle tracking in live-cell time-lapse sequences. *Nat Methods* 5(8):695–702.
31. Davies PF, et al. (1997) Spatial relationships in early signaling events of flow-mediated endothelial mechanotransduction. *Annu Rev Physiol* 59(1):527–549.
32. Xia Y, Whitesides GM (1998) Soft lithography. *Annu Rev Mater Sci* 28:153–184.
33. Krouglova T, Vercammen J, Engelborghs Y (2004) Correct diffusion coefficients of proteins in fluorescence correlation spectroscopy. Application to tubulin oligomers induced by Mg2+ and Paclitaxel. *Biophys J* 87(4):2635–2646.

Downloaded at Palestinian Territory, occupied on December 14, 2021

www.manaraa.com